

CrossMark
click for updatesCite this: *J. Mater. Chem. A*, 2015, 3, 9406Received 28th February 2015
Accepted 25th March 2015

DOI: 10.1039/c5ta01532d

www.rsc.org/MaterialsA

Radically grown obelisk-like ZnO arrays for perovskite solar cell fibers and fabrics through a mild solution process†

Sisi He,‡ Longbin Qiu,‡ Xin Fang, Guozhen Guan, Peining Chen, Zhitao Zhang and Huisheng Peng*

A general and effective strategy has been developed to fabricate both perovskite photovoltaic fibers and fabrics by synthesizing obelisk-like ZnO arrays to replace the TiO₂ layer through a mild solution process. The obelisk-like ZnO aggregates were perpendicularly grown on substrates in an aligned format and with tunable sizes, offering many advantages, such as effective penetration of a second phase into the voids with a high stability. The perovskite photovoltaic fibers and fabrics can be twisted in three dimensions without obvious damage to the structure.

Introduction

Organic–inorganic halide perovskites have emerged as a new star for the next generation photovoltaic devices.^{1,2} The power conversion efficiency of these compounds has displayed a sharp increase to approximately the same as crystal silicon-based solar cells over past five years.^{3,4} In particular, the intrinsic properties, including solid state and easy processing, offer promising applications for flexible and wearable electronic devices that represent a rapidly growing direction in multi-disciplinary fields. However, the requirement of annealing at high temperatures for the compact and mesoscopic TiO₂ layer in the typical structure has largely limited the application of perovskite solar cells, *i.e.* the commonly used flexible polymer substrates cannot survive thermal treatment at high temperatures.^{5–12} A low temperature solution process for the preparation of the TiO₂ compact and mesopore layer is also promising for efficient perovskite solar cells, although most of them were fabricated on rigid glass substrates.^{13–15} In addition, the

available flexible perovskite solar cells appear in a planar structure that can be typically bent along one direction but cannot be twisted in three dimensions.¹⁶ As a result, it is not effective for them to be used on soft and curved substrates as well as for wearable applications. Furthermore, although the flexible planar perovskite solar cells can be made to be thin, they are still relatively heavy and large, and cannot be effectively integrated into wearable and micro-electronic devices. Therefore, it is necessary to develop lightweight, three-dimensional flexible perovskite photovoltaic devices through low-cost and highly-efficient fabrication processes.

Herein, a general and effective strategy has been developed to fabricate both perovskite photovoltaic fibers and fabrics by synthesizing obelisk-like ZnO arrays to replace the TiO₂ layer through a mild solution process. Unlike traditional dye-sensitized and quantum-dot solar cells with similar structures, the perovskite layer possesses a higher light absorbing efficiency and charge carrier mobility, so the thickness of the solid-state cell can be made thinner, which is beneficial for producing flexible devices. Further, the obelisk-like ZnO aggregates are perpendicularly grown on substrates in an aligned format and with tunable sizes, providing many advantages, such as effective penetration of a second phase into the voids and rapid charge transport along their axes, which are further promoted by the high specific surface area. As a result, both the perovskite photovoltaic fibers and fabrics demonstrate high power conversion efficiencies. The perovskite photovoltaic fibers and fabrics can be twisted in three dimensions without obvious damage to the structure, and the power conversion efficiencies varied by 7% after deforming for 200 cycles.

Experimental section

Growth of the ZnO nano-obelisk array

A KOH/methanol solution (0.487 g in 23 mL) was dropped into a zinc acetate/dehydrate methanol solution (0.979 g in 42 mL) with stirring at 63 °C. After reacting for 2.5 h, the solution was cooled down to room temperature and left to stand overnight

State Key Laboratory of Molecular Engineering of Polymers, Collaborative Innovation Center of Polymers and Polymer Composite Materials, Department of Macromolecular Science and Laboratory of Advanced Materials, Fudan University, Shanghai 200438, China. E-mail: penghs@fudan.edu.cn

† Electronic supplementary information (ESI) available. See DOI: 10.1039/c5ta01532d

‡ These authors contributed equally.

prior to centrifugation. The centrifuged ZnO nanoparticles (0.356 g) were re-dispersed in a solvent mixture of chloroform (1.5 mL), isopropanol (1.5 mL) and methanol (25 mL). A substrate was then inserted into the resulting solution, followed by drying at room temperature. The synthesis of the ZnO nano-obelisks was carried out in an aqueous solution containing 0.03 M $\text{Zn}(\text{NO}_3)_2 \cdot 6\text{H}_2\text{O}$, 0.025 M $(\text{CH}_2)_6\text{N}_4$ and 0.005 M polyethyleneimine ($M_w = 1200 \text{ g mol}^{-1}$) at a temperature range of 50 to 90 °C and a time range of 5 to 120 min. The products were rinsed with deionized water three times and dried at 90 °C.

Fabrication of a fiber-shaped PSC

A stainless steel wire (diameter of 0.127 mm) was sequentially washed with acetone, isopropanol and deionized water under ultrasonic treatment for 10 min each. The synthesis of $\text{CH}_3\text{NH}_3\text{I}$ is described in the ESI.† After being modified with the aligned ZnO nano-obelisk array on the surface, the steel wire was inserted into a 1 M PbI_2 /dimethyl sulfoxide solution three times and dried at 80 °C for 30 min. The resulting fiber was soaked in a $\text{CH}_3\text{NH}_3\text{I}$ /isopropyl solution (10 mg mL^{-1}) for 10 min and annealed at 80 °C for 30 min. After cooling to room temperature, it was dropped into a hole-transporting material solution containing 2,2',7,7'-tetrakis(*N,N*-para-dimethoxyphenyl-amine)-9,9-spirobifluorene (61.4 mM), lithium bis(trifluoromethylsulfonyl)imide (26 mM), and 4-*tert*-butylpyridine (55 mM) in a mixed solvent system of chlorobenzene and acetonitrile (volume ratio of 20/1). A transparent CNT sheet was finally wrapped around the resulting wire to produce a fiber-shaped PSC. The preparation of the CNT sheet is described in the ESI.†

Results and discussion

The aligned obelisk-like ZnO arrays were synthesized through a chemical bath deposition method. Briefly, a layer of ZnO nanoparticles (5 nm in diameter) was dip-coated on the desired substrate, such as a stainless steel wire, as nucleation sites (Fig. S1 and S2†). The ZnO nano-obelisks were then perpendicularly grown on the substrate at low temperatures (60–100 °C) in an aqueous solution containing $\text{Zn}(\text{NO}_3)_2 \cdot 6\text{H}_2\text{O}$, $(\text{CH}_2)_6\text{N}_4$ and polyethyleneimine (PEI). The related reactions during the growth are listed below.¹⁷

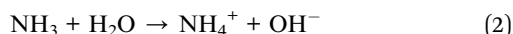


Fig. 1 shows a ZnO nano-obelisk array radically grown on a stainless steel wire with a number density of $\sim 10^{10} \text{ cm}^{-2}$ on the surface. The diameters of the nano-obelisks fluctuated around 150 nm at the bottom and gradually decreased to $\sim 70 \text{ nm}$ along the axis before a sharp tip. The ZnO nano-obelisks were stably anchored on the substrate even after bending 1000 times.

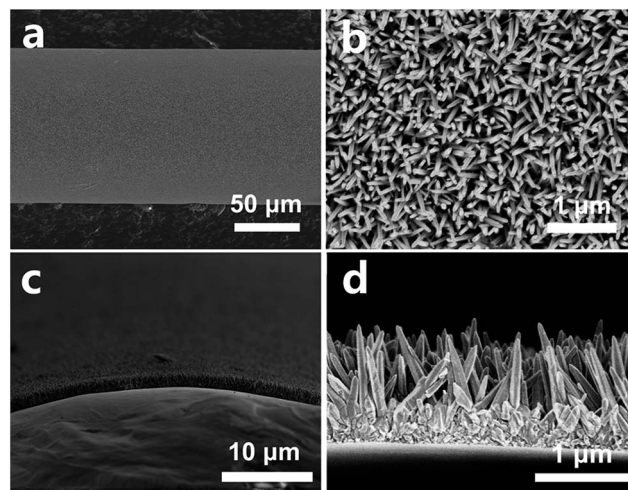


Fig. 1 SEM images of a ZnO nano-obelisk array grown on a steel wire. (a and b) Side view at low and high magnifications, respectively. (c and d) Cross-sectional view at low and high magnifications, respectively. The ZnO array was prepared at 90 °C.

Several factors exert significant impacts on the formation of the ZnO nano-obelisks. The ZnO nanoparticles act as a seed layer to initiate the radical growth of the nano-obelisks.¹⁸ In the absence of the nanoparticles, ZnO aggregates were sparsely strewn over the substrate rather than densely and perpendicularly aligned under the same growing conditions (Fig. S3†). PEI is also indispensable for a longer and thinner array. Irregular larger aggregates rather than aligned ZnO nano-obelisks were produced without the space limitation of growth with PEI (Fig. S4†).¹⁹ Thermodynamically, the crystals were inclined to grow preferentially from the high energy crystal plane, *i.e.* the (0002) plane in the ZnO material.²⁰ PEI can be absorbed onto the nonpolar side facets, making the (0002) plane favorably exposed in the solution, which was corroborated by the high-intensity (0002) diffraction peaks in the X-ray diffraction (XRD) patterns.¹⁹

Besides the ZnO seed particles, the growth of the ZnO nano-obelisks was also affected by time and temperature. Fig. S5† traces the morphology evolution of the ZnO nano-obelisks during growth. ZnO buds sprouted from the seed layer in the first 10 min. The “buds” then evolved into a nano-array in the following 20 minutes (Fig. S6†). Afterwards, the ZnO nano-obelisks grew longer with the increasing time (Fig. S7†). The temperature kinetically facilitated the growing process, and a higher temperature produced longer ZnO nano-obelisks (Fig. S7–S9†). The length distributions of the ZnO nano-obelisks grown for 90 min at different temperatures is shown in Fig. S10.† In the present study, the ZnO nano-obelisks could be obtained within a temperature window of between 60 and 90 °C. As expected, the diffraction intensities were enhanced with increasing temperature, indicating that the ZnO nano-obelisks formed better crystal structures at higher temperatures. At a lower temperature, such as 50 °C, and a higher temperature, such as 100 °C, no ZnO nano-obelisks were observed (Fig. S11 and S12†). This phenomenon

may be explained by the inhibition of nucleation and growth at lower temperatures and “Ostwald ripening” of the seed layer that aggregates into larger particles at higher temperatures.¹⁸ Importantly, the growth of nano-obelisks was imperious to the substrate and could be realized on various curved and planar substrates, such as titanium wire, copper foil and fluorine doped tin oxide glass (Fig. S13†). Unlike the previously required high temperature annealing processes for TiO₂ that might oxidize the metal substrate and deteriorate the electrode performance by reacting with the metal oxide blocking layer, this mild process does not damage the properties of substrates.²¹

The crystallinity of the nano-obelisks was analyzed by XRD spectroscopy and transmission electron microscopy (TEM). The XRD pattern shows strong and sharp characteristic diffraction peaks that indicate a hexagonal wurzite crystallite (Fig. S14†). The higher peak at 34.4° corresponds to a (0002) plane, suggesting that the nano-obelisks were grown along the [0001] direction with their *c*-axis perpendicular to the substrate.²² The TEM image and corresponding electron diffraction pattern in Fig. S15† also back up this conclusion. The formation of sharp tips on the ZnO nano-obelisks is related to the variation in Zn²⁺ concentration during growth. When the Zn²⁺ ions are depleted in the solution, the crystal growth tends to slow down, which differentiates the growing rates between the plane center and boundary. A sharp tip is formed when the center grows faster than the boundary with increasing growth time (Fig. S16†).²³

The unique one-dimensional structure and mild growing conditions make the ZnO nano-obelisks applicable in flexible photovoltaic devices. A fiber-shaped perovskite solar cell (PSC) was then fabricated using the aligned ZnO nano-obelisks as an effective electron transport layer. The light-harvesting perovskite and hole conductors were successively impregnated on the ZnO nano-obelisk scaffold that was prepared on a steel wire. Carbon nanotube (CNT) sheets, which are conductive and transparent, were wrapped on the outside as the back contact electrode (Fig. 2a and S17†).²⁴

The CH₃NH₃PbI₃ perovskite layer was prepared through a two-step dip-coating process. PbI₂ was first dissolved in dimethyl sulfoxide and then dip-coated onto the ZnO nano-obelisk array to form a thin and dense layer (Fig. S18†).²⁵ The as-prepared CH₃NH₃PbI₃ crystals typically had a cubic structure and their sizes were decreased when CH₃NH₃I concentrations were increased from 4 to 10 mg mL⁻¹ (Fig. S19†, 2c and 2d).²⁶ It should be noted that the size of CH₃NH₃PbI₃ should be compatible with the ZnO scaffold. When the CH₃NH₃PbI₃ crystals were too large, the ZnO nano-obelisks were prone to collapsing, resulting in short circuits and poor performances of the solar cell (Fig. S20†). Therefore, in the present study, a uniform CH₃NH₃PbI₃ capping layer was prepared from a 10 mg mL⁻¹ CH₃NH₃I solution and infiltrated into the voids of the ZnO obelisk array (Fig. 2c and d). The complete structure of this perovskite solar cell fiber is shown in Fig. S21,† with a thickness of ~150 nm for the perovskite capping layer and 350 nm for the hole transport layer.

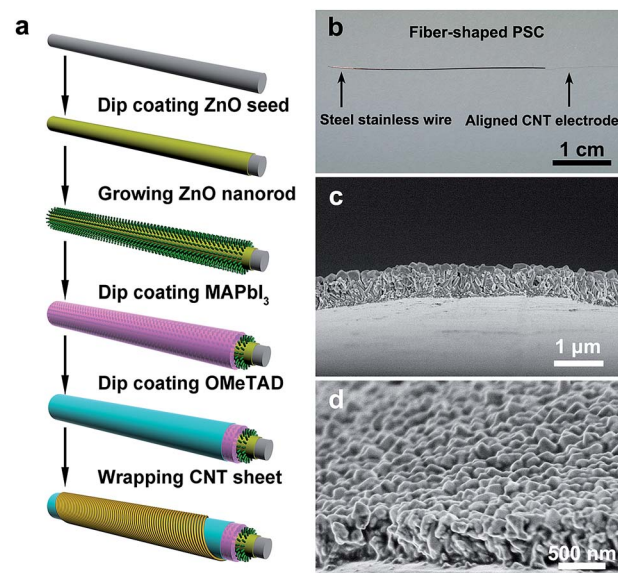


Fig. 2 Fiber-shaped PSC based on the aligned ZnO nano-obelisks. (a) Schematic illustration showing the fabrication process. (b) Photograph of a fiber-shaped PSC. (c and d) SEM images of a perovskite layer on the ZnO nano-obelisk array at low and high magnifications, respectively. The CH₃NH₃I concentration was 10 mg mL⁻¹.

Fig. 3a displays the current density–voltage (*J*–*V*) curves of fiber-shaped PSCs containing ZnO nano-obelisks with different lengths. The comparison revealed that the 700 nm ZnO nano-obelisks provided the solar cell with the highest power conversion efficiency of 3.8%, which was due to a compromise between the surface area and the charge recombination. This value is higher than the value for flexible perovskite solar cells based on ZnO nanorods fabricated on planar polymer substrates, which exhibit a power conversion efficiency of 2.61% with an open-circuit voltage of 0.8 V, short-circuit current density of 7.52 mA cm⁻² and fill factor of 0.43.²⁹ Longer obelisks with higher surface areas can absorb more perovskite materials but they increase the pathways for charge transport with more charge recombination. In contrast, shorter obelisks can reduce the charge recombination while also decreasing the surface area.

To highlight the merit of the nano-obelisk morphology, a ZnO seed layer and a nanorod array were also introduced as electron transport layers to fabricate fiber-shaped PSCs under the same conditions. As a small amount of perovskite was attached to the ZnO seed layer, the resulting PSC produced a much lower *J*_{SC} value of 3.72 mA cm⁻² and a power conversion efficiency of 0.98% (Fig. S22 and S23†). In the case of the ZnO nanorod array, the perovskite could not be fully infiltrated into the voids, which engendered a severe charge recombination, leading to an inferior power conversion efficiency of 1.0% (Fig. S24 and S25†).^{27–29} Due to a coaxial structure, the photovoltaic performance of the fiber-shaped PSC was insusceptible to the angle of incident light (Fig. 3c). As the ZnO nano-obelisk array was firmly anchored on the fiber substrate, the fiber-shaped PSC was flexible and could be bent without fatigue. The power conversion efficiency was

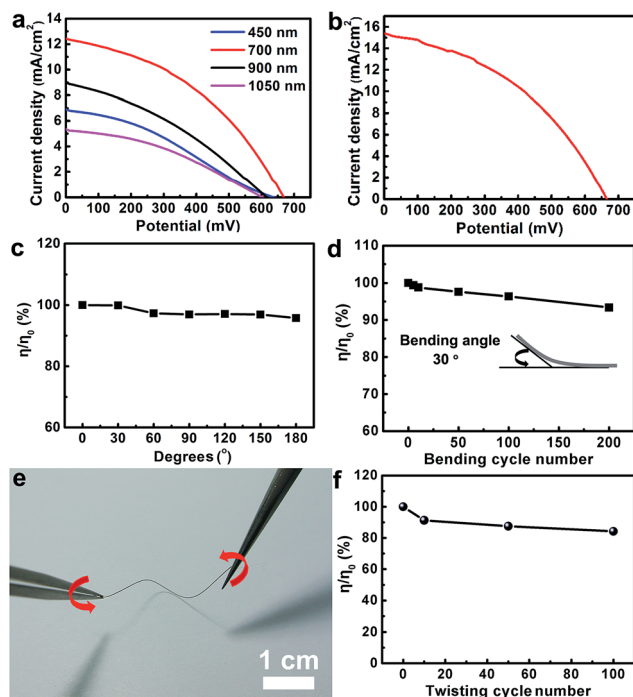


Fig. 3 Photovoltaic performances of the fiber-shaped PSCs. (a) J - V curves of the fiber-shaped PSCs with different lengths of ZnO nano-obelisks. (b) J - V curve of the optimized fiber-shaped PSC. (c) Dependence of the power conversion efficiency on the angle of incident light. η_0 and η correspond to the power conversion efficiencies at 0° and the other angle, respectively. (d) Dependence of the power conversion efficiency on the bending number. η_0 and η correspond to the power conversion efficiencies before and after bending for different times, respectively. (e) Photograph of a perovskite solar cell fiber under twisting. (f) Dependence of the power conversion efficiency on the twisting cycle number. η_0 and η correspond to the power conversion efficiencies before and after twisting for different times, respectively.

maintained at 93% after bending for 200 cycles (Fig. 3d). The stability in the power conversion efficiency upon bending is comparable to the flexible planar counterpart, where a decrease of $\sim 7\%$ was observed.¹⁶ In particular, the fiber shape offered a unique capability for three-dimensional deformations, such as twisting, that are generally unavailable for conventional planar solar cells. The power conversion efficiency was maintained at 84% after twisting with a twisting angle of 30° (Fig. 3e and f). Note that here the piezoelectric dipole may also slightly contribute to enhancing the power conversion efficiency of the fiber-shaped perovskite solar cell based on the ZnO array under deforming conditions due to the increased built-in electric field that enhanced the charge separation and transport.^{30,31}

Based on a similar strategy, a ZnO nano-obelisk array was also grown on a fabric substrate, such as a steel fabric (Fig. 4). As a result, an all-solid-state PSC fabric with a stable performance can be developed through the method described above (Fig. S26[†]). As expected, this photovoltaic fabric was also flexible and could be bent for hundreds of cycles without obvious damage to the structure.

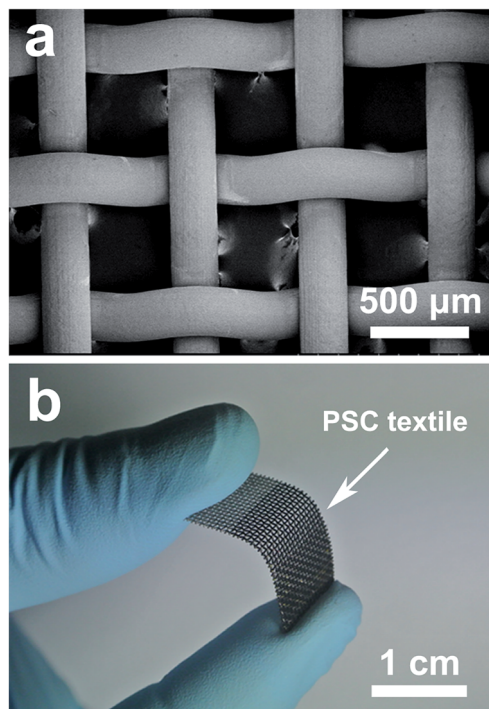


Fig. 4 (a) SEM image of the ZnO nano-obelisk array grown on a stainless steel fabric. (b) Photograph of the PSC fabric.

Conclusion

In conclusion, we have synthesized a new family of obelisk-like ZnO arrays through a low-temperature and solution-based process. The mild growing conditions make the ZnO nano-obelisk array compatible with various flexible polymer substrates that are highly desired for flexible photovoltaic devices. As a promising application, the ZnO nano-obelisk array has been introduced as the electron transport layer to make novel PSCs in both fiber and fabric formats. This work also provides a general and effective strategy for the structure control of nanomaterials for electronic and energy devices.

Acknowledgements

This work was supported by MOST (2011CB932503), NSFC (21225417), STCSM (12nm0503200), the Fok Ying Tong Education Foundation, the Program for Special Appointments of Professors at Shanghai Institutions of Higher Learning, and the Program for Outstanding Young Scholars from the Organization Department of the CPC Central Committee.

References

- W. Nie, H. Tsai, R. Asadpour, J. C. Blancon, A. J. Neukirch, G. Gupta, J. J. Crochet, M. Chhowalla, S. Tretiak, M. A. Alam, H. L. Wang and A. D. Mohite, *Science*, 2015, **347**, 522–525.
- D. Shi, V. Adinolfi, R. Comin, M. Yuan, E. Alarousu, A. Buin, Y. Chen, S. Hoogland, A. Rothenberger, K. Katsiev,

- Y. Losovyj, X. Zhang, P. A. Dowben, O. F. Mohammed, E. H. Sargent and O. M. Bakr, *Science*, 2015, **347**, 519–522.
- 3 A. Kojima, K. Teshima, Y. Shirai and T. Miyasaka, *J. Am. Chem. Soc.*, 2009, **131**, 6050–6051.
- 4 N. J. Jeon, J. H. Noh, W. S. Yang, Y. C. Kim, S. Ryu, J. Seo and S. I. Seok, *Nature*, 2015, **517**, 476–480.
- 5 J. Burschka, N. Pellet, S. J. Moon, R. Humphry-Baker, P. Gao, M. K. Nazeeruddin and M. Grätzel, *Nature*, 2013, **499**, 316–319.
- 6 M. M. Lee, J. Teuscher, T. Miyasaka, T. N. Murakami and H. J. Snaith, *Science*, 2012, **338**, 643–647.
- 7 H. S. Kim, C. R. Lee, J. H. Im, K. B. Lee, T. Moehl, A. Marchioro, S. J. Moon, R. Humphry-Baker, J. H. Yum, J. E. Moser, M. Grätzel and N. G. Park, *Sci. Rep.*, 2012, **2**, 591.
- 8 D. Y. Liu and T. L. Kelly, *Nat. Photonics*, 2014, **8**, 133–138.
- 9 J. M. Ball, M. M. Lee, A. Hey and H. J. Snaith, *Energy Environ. Sci.*, 2013, **6**, 1739.
- 10 K. Wojciechowski, M. Saliba, T. Leijtens, A. Abate and H. J. Snaith, *Energy Environ. Sci.*, 2014, **7**, 1142.
- 11 J. You, Z. Hong, Y. M. Yang, Q. Chen, M. Cai, T. B. Song, C. C. Chen, S. Lu, Y. Liu, H. Zhou and Y. Yang, *ACS Nano*, 2014, **8**, 1674–1680.
- 12 J. Y. Jeng, Y. F. Chiang, M. H. Lee, S. R. Peng, T. F. Guo, P. Chen and T. C. Wen, *Adv. Mater.*, 2013, **25**, 3727–3732.
- 13 J. T.-W. Wang, J. M. Ball, E. M. Barea, A. Abate, J. A. Alexander-Webber, J. Huang, M. Saliba, I. Mora-Sero, J. Bisquert, H. J. Snaith and R. J. Nicholas, *Nano Lett.*, 2014, **14**, 724–730.
- 14 K. Wojciechowski, M. Saliba, T. Leijtens, A. Abate and H. J. Snaith, *Energy Environ. Sci.*, 2014, **7**, 1142–1147.
- 15 H. Zhou, Q. Chen, G. Li, S. Luo, T. B. Song, H. S. Duan, Z. Hong, J. You, Y. Liu and Y. Yang, *Science*, 2014, **345**, 542–546.
- 16 B. J. Kim, D. H. Kim, Y.-Y. Lee, H.-W. Shin, G. S. Han, J. S. Hong, K. Mahmood, T. K. Ahn, Y.-C. Joo, K. S. Hong, N.-G. Park, S. Lee and H. S. Jung, *Energy Environ. Sci.*, 2015, **8**, 916–921.
- 17 L. N. Dem'yanets, D. V. Kostomarov and I. P. Kuz'mina, *Inorg. Mater.*, 2002, **38**, 124–131.
- 18 C. Pacholski, A. Kornowski and H. Weller, *Angew. Chem., Int. Ed.*, 2002, **41**, 1188–1191.
- 19 S. Xu and Z. L. Wang, *Nano Res.*, 2011, **4**, 1013–1098.
- 20 D. He, X. Sheng, J. Yang, L. Chen, K. Zhu and X. Feng, *J. Am. Chem. Soc.*, 2014, **136**, 16772–16775.
- 21 Y. Zhu, L. Zhang, L. Wang, Y. Fu and L. Cao, *J. Mater. Chem.*, 2001, **11**, 1864–1868.
- 22 L. Vayssieres, *Adv. Mater.*, 2003, **15**, 464–466.
- 23 A. Moulahi and F. Sediri, *Mater. Res. Bull.*, 2013, **48**, 3723–3728.
- 24 L. Qiu, J. Deng, X. Lu, Z. Yang and H. Peng, *Angew. Chem., Int. Ed.*, 2014, **53**, 10425–10428.
- 25 Y. Z. Wu, A. Islam, X. D. Yang, C. J. Qin, J. Liu, K. Zhang, W. Q. Peng and L. Y. Han, *Energy Environ. Sci.*, 2014, **7**, 2934–2938.
- 26 J. H. Im, I. H. Jang, N. Pellet, M. Grätzel and N. G. Park, *Nat. Nanotechnol.*, 2014, **9**, 927–932.
- 27 M. H. Kumar, N. Yantara, S. Dharani, M. Graetzel, S. Mhaisalkar, P. P. Boix and N. Mathews, *Chem. Commun.*, 2013, **49**, 11089–11091.
- 28 Y. Zhao and K. Zhu, *J. Phys. Chem. Lett.*, 2013, **4**, 2880–2884.
- 29 D. Liu, J. Yang and T. L. Kelly, *J. Am. Chem. Soc.*, 2014, **136**, 17116–17122.
- 30 C. Xu and Z. L. Wang, *Adv. Mater.*, 2011, **23**, 873–877.
- 31 C. Xu, X. Wang and Z. L. Wang, *J. Am. Chem. Soc.*, 2009, **131**, 5866–5872.